Article

Whole CNS 3D Cryo-fluorescence Tomography Shows CSF Clearance along Nasal Lymphatics, Spinal Nerves, and Lumbar/Sacral Lymph Nodes

Christian Stokes[1], Eli F White[1], Steve Toddes[1], Nicole Bens[2], Praveen Kulkarni[2], Craig F Ferris[2,*]

[1] EMIT Imaging, Baltimore MD
[2] Center for Translational NeuroImaging, Northeastern University, Boston, MA 02115, USA
*Corresponding author: c.ferris@northeastern.edu; Tel.: 508 259 4908

Abstract: Unwanted proteins and metabolic waste in cerebral spinal fluid are cleared from the brain by meningeal and nasal lymphatics, and perineural sheath of cranial nerves; however, the distribution and clearance of CSF along the subarachnoid space of the entire spinal cord is not fully understood. It was hypothesized that the anatomical resolution of Cryo-Fluorescence Tomography (CFT) could provide the visual evidence of clearance across the spinal cord at each level of the vertebral column. To that end, isoflurane anesthetized mice were infused into the lateral cerebroventricle with 5.0 µl of quantum dots [QdotR 605 ITKTM amino (PEG)] over two mins. Mice were allowed to recover (ca 2-3 min) and remained awake and ambulatory for 5, 15, 30, 60 and 120 minutes after which they were euthanized, and the entire intact body frozen at -80^0. The entire mouse was sectioned and imaged to produce an isotropic voxel resolution of 35 µm. Both white light and fluorescent images were captured after each slice to produce high resolution three-dimensional volumes for each mouse. CFT highlighted the circulation of tracer throughout the ventricular system and central canal of the spinal cord and the entire subarachnoid space of the CNS. Signal could be visualized in the nasal cavity, deep cervical lymph nodes, thoracic lymph nodes and more superficial submandibular lymph nodes as early as 15 min post infusion. Fluorescent signal could be visualized along the dorsal root ganglia and down the proximal extension of the spinal nerves of the thoracic and lumbar segments at 30 min. There was significant accumulation of tracer in the lumbar and sacral lymph nodes between 15- 60 min. The dense fluorescent signal in the thoracic vertebrae noted at 5- and 15-mins post infusion was significantly reduced by 30 min. Indeed, all signal in the spinal cord was ostensibly absent by 120 min except for trace amounts in the coccyx. The brain still had some residual signal at 120 min. These data show that Qdots with a hydrodynamic diameter of 16-20 nm rapidly clear from the brain of awake mice. These data also clearly demonstrate the rapid distribution and efflux of trace along a major length of the vertebral column and the potential contribution of the spinal cord in the clearance of brain waste.

Keywords: brain clearance; Qdots; nasal turbinates; subarachnoid space; cervical lymphatics; sympathetic ganglia; cervical spinal cord; thoracic spinal cord

1. Introduction

The subject of cerebral spinal fluid (CSF) clearance, it routes and mechanisms in health and disease has garnered much attention particularly with respect to aging and neurodegeneration (1). How does metabolic waste and unwanted proteins generated at the level of neurovascular unit in brain parenchymal interstitial fluid find its way out? There is evidence that clearance occurs as interstitial fluid moves along paravascular and perivascular routes accumulating as CSF in the subarachnoid space (SAS) to leave through nasal and meningeal pathways and perineural sheaths. (2-4).

It is well documented that CSF drains from the SAS through the cribriform plate along olfactory nerves to the nasal mucosa lining the nasal turbinates and from there

Preprints (www.preprints.org) | NOT PEER-REVIEWED | Posted: 9 November 2022 doi:10.20944/preprints202211.0171.v1

through nasal lymphatics to the deep cervical lymph nodes (5-7). There is also a direct route of CSF clearance to the deep cervical lymph nodes via lymphatic vessels located in the meninges along the ventral surface of the brain in mice (8, 9). While less emphasized, there is evidence from early studies using horse radish peroxidase (HRP) of tracer appearing in the lumen of cerebral blood vessels suggesting a direct clearance of brain CSF into the general circulation (10, 11), a finding advanced by Lam et al. at the level of the spinal cord (12). Indeed, the spinal cord itself is reported to have a significant role in the clearance of CSF via meningeal lymphatics and perineuronal sheaths (13, 14).

Most recently, Leaston et al., reported a novel pathway by which waste from the brain to the nasal mucosa enters the nasal pharynx to ultimately be swallowed (15). This finding was confirmed in two studies, one using magnetic resonance imaging to follow ferumoxytol circulation and clearance from the brain in awake rats during the imaging session, and a second using Qdot fluorescence microscopy of the *ex vivo* esophagus. Within 10-15 min after intracerebroventricular (ICV) infusion, tracer from both studies can been seen outside the brain along the nasopharynx and esophagus. Indeed, this finding was the motivation behind these studies in mice. Using 3D cryofluorescent tomography (CFT) we hoped to see the accumulation over time of ICV administered Qdots in the stomach and intestine of mice. Unfortunately, due to the background autofluorescence, particularly in the gastrointestinal tract this was not possible. Instead, we were able to create a time series showing the distribution, localization, and clearance of Qdot fluorescence over the entire brain and spinal cord and associated lymphatic nodes. These data are presented and discussed with an emphasis on the spinal cord as a route CSF clearance.

2. Methods and Materials

2.1. Animal usage

Male C57BL/J6 mice (n = 5) approximately 100 days of age and weighing between 28-30 gm were obtained from Charles River Laboratories (Wilmington, Massachusetts, USA). Mice were maintained on a 12:12 hour light-dark cycle with lights on at 07:00 hours and allowed access to food and water ad libitum. All mice were acquired and cared for in accordance with the guidelines published in the Guide for the Care and Use of Laboratory Animals (National Institutes of Health Publications No. 85–23, Revised 1985) and adhered to the National Institutes of Health and the American Association for Laboratory Animal Science guidelines. The protocols used in this study complied with the regulations of the Institutional Animal Care and Use Committee at the Northeastern University and adhere to the ARRIVE guidelines for reporting *in vivo* experiments in animal research (16)

2.2. Quantum dot infusion

Quantum dots [QdotR 605 ITKTM amino (PEG)] with a hydrodynamic diameter of 16–20 nm were obtained from Thermo Fisher Scientific (Waltham MA, USA). Qdots were diluted 1/100 in sterile saline prior to infusion. While under isoflurane anesthesia (unresponsive to foot pinch, 40-45 breathes/min) the skin was incised and skull over bregma exposed. A 30-gauge needle connected to a 200 µl syringe was directed toward the lateral cerebroventricle (stereotaxic coordinates: 0.50 mm rostral to bregma, 1.0 mm lateral to midsagittal suture, and 3.5 mm down from the skull surface). Five µl of Qdots were infusion over two minutes. Mice were treated with buprenorphine (1.5 mg/kg) and the open skin repaired with surgical glue. Mice were allowed to recover from anesthesia; usually ambulatory by 2-3 mins. At time intervals of 5, 15-, 30-, 60- and 120-minutes post recovery, mice were sacrificed with Euthasol® (150 mg/kg, IP) and the entire body laid out in a prone position on aluminum foil and placed in a -80^0 refrigerator. These specimens were then shipped frozen on dry ice to Emit Imaging (Baltimore, MD).

2.3. Cryo-fluorescence Tomography (CFT)

The animals were imaged on Emit Imaging's Xerra platform at a 35µm isotropic voxel resolution. The Xerra is an automated CFT platform with an integrated cryomicrotome

Preprints (www.preprints.org) | NOT PEER-REVIEWED | Posted: 9 November 2022 doi:10.20944/preprints202211.0171.v1

and proprietary software, that captures 2D white light and fluorescent images of *ex vivo* serial sections and compiles them into 3D images. Sample preparation involved freezing five mice in a block of O.C.T (Ultrafreeze OCT Clear, Cancer Diagnostics Durham, NC, USA). The block with a field of view of 17cm x 10 cm was then placed in the Xerra and the mice were then automatically sectioned in 35um slices over 17 hr at -15^{0}C. The newly exposed block face was then imaged for white light, as well as fluorescence signal, while the shaved tissue was discarded. 16-bit fluorescence images were acquired with consistent exposure times of 5 ms, 50 ms, 500 ms, 1500 ms and 2500 ms. These images were then combined into a single 32-bit high dynamic range (HDR) image to extend the Xerra's detection limits beyond a single exposure. Exposure times and illumination levels were fixed through the imaging of each animal to ensure sample to sample consistency.

3. Results

Shown in **Fig 1** are CFT images of the CNS taken at different time intervals following the recovery from the infusion of Qdots into the lateral cerebroventricle. Highlighted are the different segments of the vertebral column e.g., cervical, thoracic, lumbar, sacral and coccyx. Note the distribution of fluorescence across much of the vertebral column within 5 min of recovery. Fluorescence can be observed in the most rostral part of the image in what is the nose of the mouse filling the nasoturbinates (NT). At 15 min signal can also be seen in the most caudal part of the image at the coccyx, the end of the vertebral column at the hind end of the mouse (see **Fig 2**). The submandibular lymph nodes (smLN) accumulate Qdots at 15 min that persists for up to 60 min but is absent by 120 min. By 60 min the entire vertebral column is heavily penetrated by Qdots (see **Fig 3**) that is all but absent by 120 min.

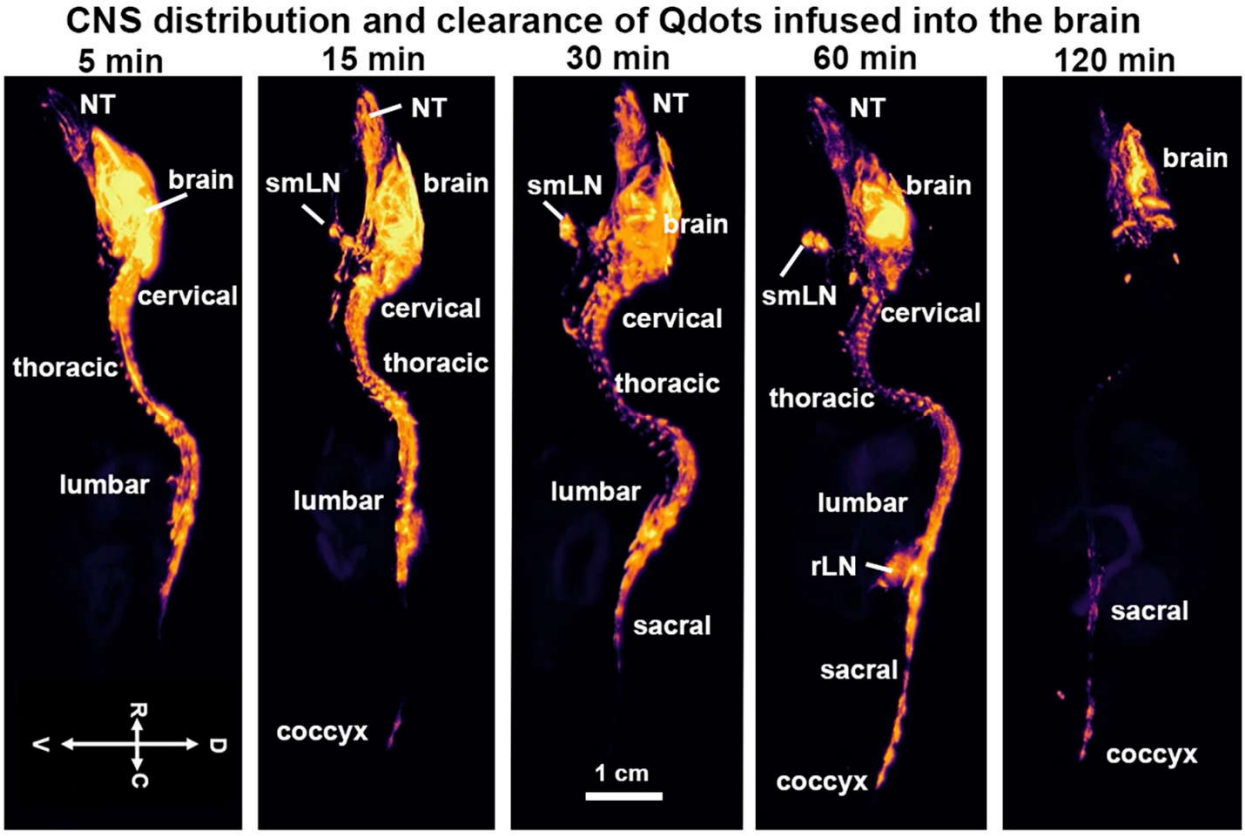

Figure 1. CNS distribution and clearance time series**.** Shown are cryo-fluorescent microscopic images of the CNS taken at different time intervals following the infusion of into the lateral cerebroventricle. Highlighted are the different segments of the vertebral column e.g., cervical, thoracic, lumbar, sacral and coccyx. Abbreviations: NT – nasoturbinates; rLN - renal lymph nodes; smLN – submandibular lymph nodes. Scale bar 1 cm.

Preprints (www.preprints.org) | NOT PEER-REVIEWED | Posted: 9 November 2022 doi:10.20944/preprints202211.0171.v1

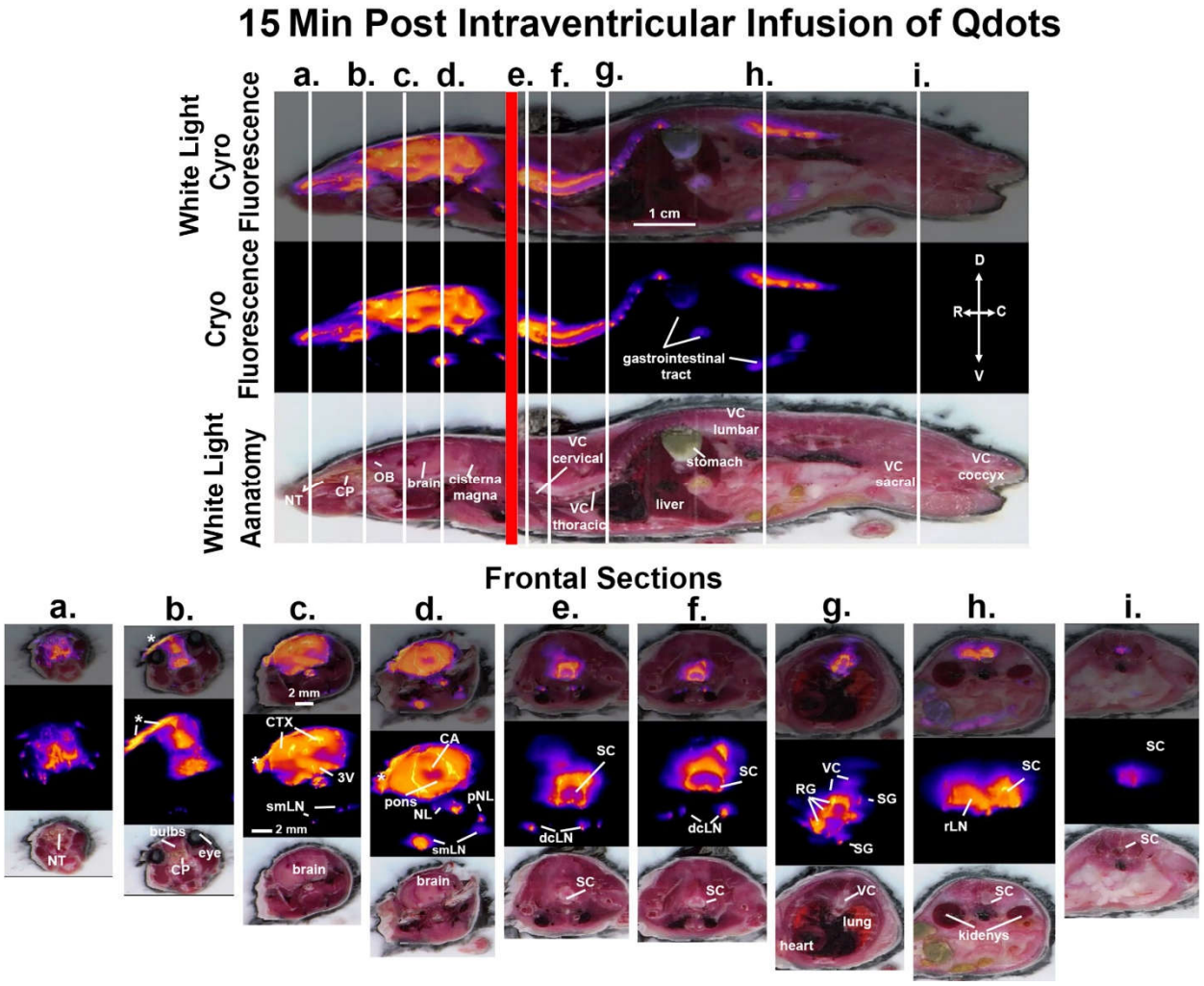

Figure 2. CNS distribution and clearance at 15 min**.** Scheme 15. min. post infusion of ICV Qdots. The head of the mouse and the body were not in-plane hence the red line demarking the intersection of the separate images. The perpendicular white lines labeled (a.- i.) denote the position of the frontal sections shown below. Abbreviations: NT nasoturbinates; CP - cribriform plate; CTX - cortex; 3V - third ventricle; smLN - submandibular lymphatic nodes; CA - cerebral aqueduct; NL - nasal lymphatics; pNL - parotid lymphatic nodes; SC - cervical spinal cord; dcLN - deep cervical lymph nodes; VC - thoracic vertebra; RG - root ganglia; SG - sympathetic ganglia; rLN - renal lymph nodes. Scale bar for sagittal sections 1 cm Scale bar for frontal section 2 mm.

Preprints (www.preprints.org) | NOT PEER-REVIEWED | Posted: 9 November 2022 doi:10.20944/preprints202211.0171.v1

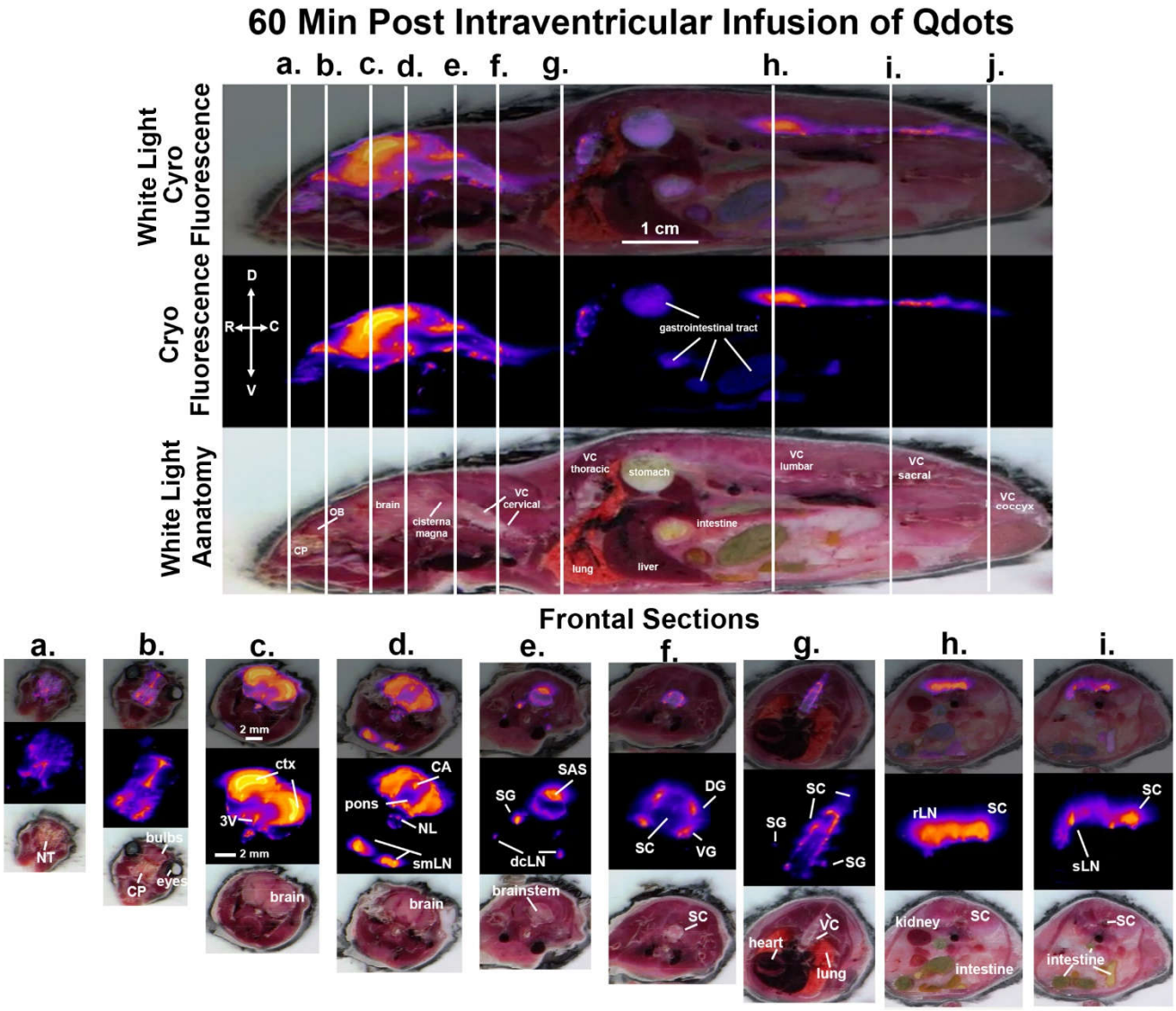

Figure 3. CNS distribution and clearance at 60 min**.** Shown above are sagittal sections depicting the same mouse imaged for white light anatomy, cryofluorescence and both together at 60 min post infusion of ICV Qdots. The perpendicular white lines labeled (a.- i.) denote the position of the frontal sections shown below. Abbreviations same as Fig 2. OB - olfactory bulbs; SAS - subarachnoid space; DG - dorsal root ganglia; VG – ventral root ganglia: laLN - aortic lymph nodes. Scale bar 1 cm and 2 mm sagittal and horizontal sections, respectively.

Shown in **Fig 2** are sagittal sections depicting the same mouse imaged for white light cryo-fluorescence and both together. The head of the mouse and the body were not in-plane hence the red line demarking the intersection of the separate images. The perpendicular white lines labeled (a.- i.) denote the position of the frontal sections shown below. Section (a.) shows fluorescent signal in the nose of the mouse localized to the nasoturbinates (NT). Section (b.) shows signal at the level of the olfactory bulbs and the underlying cribriform plate (CP). The asterisk identifies accumulation of Qdots along the surface of the skull that leaked from the infusion needle. Section (c.) depicts signal throughout the brain particularly concentrated in the cortex (CTX) and along the third ventricle (3V). Fluorescence signal is also starting to appear in the submandibular lymphatic nodes (smLN). Section (d.) shows signal in the brain at the level of the pons. The cerebral aqueduct (CA) is highlighted along with signal in the smLN and what could be identified as the nasal lymphatics (NL) and putative parotid lymphatic nodes (pNL). Section (e.) shows a section of the cervical spinal cord (SC) and the underlying deep cervical lymph nodes (dcLN).

Preprints (www.preprints.org) | NOT PEER-REVIEWED | Posted: 9 November 2022 doi:10.20944/preprints202211.0171.v1

Section (f.) shows a similar image of the cervical SC just rostral to thoracic cavity. Section (g.) shows several thoracic vertebrae (VC) and signal intensity along the root ganglia (RG) and smaller areas of signal accumulation in what would be the putative sympathetic ganglia (SG). Section (h.) shows lumbar spinal cord and the adjacent renal lymph nodes (rLN) identified by their proximity to the kidneys as shown below in the light field anatomy. The most caudal section (I.) depicts the signal in the spinal cord coccygeal region of the vertebral column.

Shown in **Fig 3** above are sagittal sections depicting the same mouse imaged for white light anatomy, cryo-fluorescence and both together. The cryofluourescent image shows autofluorescence associated with gastrointestinal tract. The perpendicular white lines labeled (a.- i.) denote the position of the frontal sections shown below. Section (a.) shows fluorescent signal in the nose of the mouse localized to the nasoturbinates. Section (b.) shows signal at the level of the olfactory bulbs (OB) and the underlying cribriform plate. Section (c.) depicts signal intensity localized primarily to the cortex of the brain and along the third ventricle (3V). Section (d.) shows signal in the brain at the level of the pons with the highest intensity in the cortex and cerebral aqueduct. Below are the submandibular lymph nodes and the putative nasal lymphatic vessels (NV). Section (e.) shows a section of the brainstem and overlying subarachnoid space (SAS). The small signal intensity comes from what we interpret as the putative sympathetic ganglia and below that are the deep cervical lymph nodes. Section (f.) shows the cervical spinal cord proximal to the thoracic cavity. The four point of signal intensity are the putative dorsal (DG) and ventral (VG) ganglia. Section (g.) shows several thoracic vertebrae and the spinal cord. The small points of signal intensity are the putative sympathetic ganglia (SG). Section (h.) shows lumbar spinal cord and the adjacent renal lymph nodes. The caudal section (I.) depicts the signal in the spinal cord and the adjacent sacral lymph nodes (sLN). Section (j.) shows the coccygeal region of the vertebral column.

Shown in **Fig 4** are fluorescence images taken of thoracic spinal cord 15 post ICV infusion of Qdots. The images highlight not only the rapid distribution of the tracer down the subarachnoid space but its egress to putative spinal lymphatic nodes, spinal nerves, and thoracic lymph node.

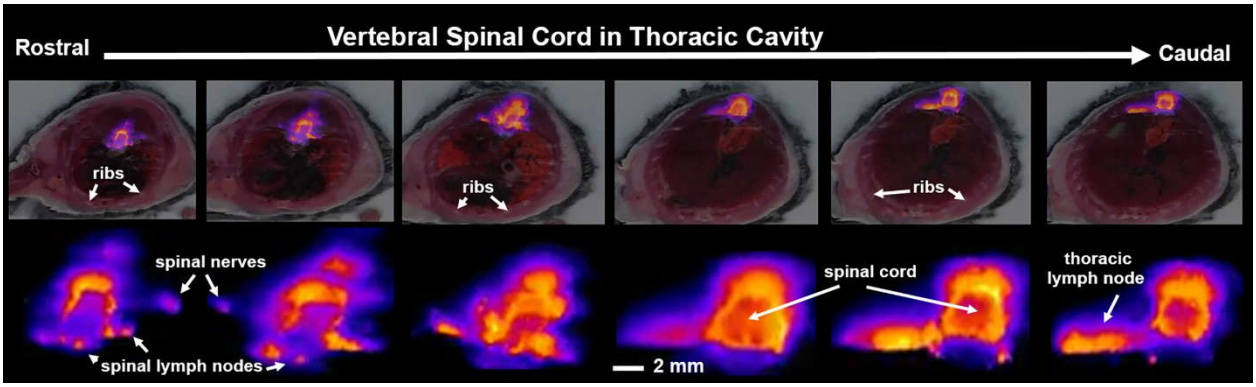

Figure 4. Distribution and clearance along thoracic spinal cord. Shown above are serial frontal sections of white light anatomy and cryo-fluorescence at the level of the vertebral spinal cord acquired 15 min post infusion of Qdots ICV (scale Magnified images of the fluorescent signal at each segment of the spinal cord are shown below (scale bar 2 mm).

4. Discussion

These studies using CFT together with white light anatomy enabled us to follow the distribution, localization, and clearance of Qdot over the entire CNS. Cifuentes and coworkers provided clear evidence in rats of the rapid movement of CSF from the lateral cerebroventricle down the central canal of the spinal cord. By 20 min after the ventricular infusion of HRP tracer reached a maximum across all segments of the spinal cord that decreased sharply by 1 hr and was cleared by 2 hr (10). In a comprehensive study, Ma and

Preprints (www.preprints.org) | NOT PEER-REVIEWED | Posted: 9 November 2022 doi:10.20944/preprints202211.0171.v1

coworkers used near-infrared and Gd based MRI contrast agents infused ICV in anesthetized and awake mice and reported movement down the central canal and subarachnoid space of the spinal cord to leave predominantly at the sacral level through lymphatic vessels leading to sacral/iliac lymph nodes (13). In their study the distribution of fluorescent tracer at the level of the thoracic spinal cord was apparent by 30 min in awake mice but delayed with anesthesia. In the present study using CFT with Qdots, the distribution of fluorescence around the thoracic spinal cord and it associated spinal lymphatic nodes and nerves could be viewed as early as 15 min post ICV infusion (see **Fig 4**).

The rapid distribution and clearance across the entire CNS could be explained in part by the chemistry of Qdots and experimental conditions, i.e., mice were studied during the light phase of the L-D cycle and while fully awake. In a previous study we reported efflux of MRI contrast agent infused IVC was under circadian control (17). The efflux of contrast agent was highest during the light phase and lowest during the dark phase in fully awake rats. The mice in this study were awake and ambulatory with mins of ICV infusion. Indeed, others have reported rapid clearance in awake mice following ICV infusion of tracer is significantly delayed under anesthesia (18, 19).

The rapid appearance of Qdots in the submandibular lymph nodes corroborates an earlier study by Mathieu et al using Qdots with an emission spectrum of 655 and having a hydrodynamic diameter ca. 19 nm similar to that used in our study (20). Infusion of 3 µl of Qdots into the cisterna magna of mice following by *in vivo* hyperspectral imaging showed fluorescence signal in the submandibular lymph nodes as early as 20 min with maximum fluorescence by 40 min. Interestingly, this *in vivo* imaging study showed preferential clearance to the submandibular lymph nodes and not the deep cervical lymph nodes highlighted by other studies (21). This finding maybe be due to the size and chemistry of the Qdots that favor this route of clearance. Using near-infrared fluorescence imaging in awake mice Ma et al., showed rapid accumulation in the submandibular lymph nodes peaking at 30 min and rapidly decreasing by 60-90 min (18). This submandibular route of CSF clearance has been attributed to clearance along the optic nerves and orbital connective tissue.

Our study shows a rapid global distribution and sustained localization of fluorescence signal over the entire brain and spinal cord that peaks as early as 30 min post ICV infusion but is almost eliminated by 120 min. This raises an important question that has been addressed at the level of the brain but not fully considered across the entire spinal cord – how does it get out? This question was addressed by Liu et al looking at the distribution of fluorescent tracer infused into white and gray matter at the level of thoracic spinal cord in rats (22). Tracer accumulated along the microvasculature i.e., arterioles, capillaries, and venules, adding the spinal cord to a body of literature that clearance of waste from interstitial fluid is carried along paravascular/perivascular routes. Waste from these microvascular routes can mix with the CSF in the meninges surround the cord and be cleared via spinal lymphatic vessels (23-25). Indeed, we were able to visual putative lymphatic nodes along spinal cord in the cervical and thoracic sections with CFT. Studies in humans report CSF flow along the lumbar nerves following intrathecal injection of tracers into the subarachnoid space (26, 27). Bechter et al., reported the rate of CSF flow to be 10 cm/hr noting the outflow from the lumbar spinal cord was remarkable (27).

Images collected with CFT providing 35 µm isotropic resolution across the entire CNS were not able to provide the needed resolution to clearly identify lymphatic vessels, nodes, nerves, and ganglia (see **Fig 4**) associated with the spinal as reported in other publications using different fluorescence microscopic procedures and histological preparations (13, 28). iDISCO with light sheet fluorescence microscopy (iDISCO/LSFM) provides exquisite detail 3D reconstructions of lymphatic vessels associated with the cervical /thoracic spinal cord of mice. The imaging modality is limited to samples of less than 1.5 cm^3 and thereby unable to capture the whole CNS transport and clearance as shown here (25). Moreover, iDISCO/LSFM is labor intensive with respect to the weeks needed to for tissue preparation and chemistry, image acquisition and analysis. The major advantage of cryofluorescence tomography is the simplicity and ability to image the entire animal. In this

study, CFT imaging allowed determination and analysis of the biodistribution of waste clearance along nasal lymphatics, spinal nerves, and vertebral lymphatics.

Author Contributions: Experimental design and manuscript preparation - PK, CFF, NB; Data generation and analysis – CS, EW, ST, NB.

Funding: Support for this project was provided by Emit Imaging.

Acknowledgments: None.

Conflicts of Interest: CS, EW and ST hold equity positions in Emit Imaging.

References

1. H. Benveniste, H. Lee, N. D. Volkow, The Glymphatic Pathway: Waste Removal from the CNS via Cerebrospinal Fluid Transport. *The Neuroscientist : a review journal bringing neurobiology, neurology and psychiatry* **23**, 454-465 (2017).
2. S. T. Proulx, Cerebrospinal fluid outflow: a review of the historical and contemporary evidence for arachnoid villi, perineural routes, and dural lymphatics. *Cell Mol Life Sci* **78**, 2429-2457 (2021).
3. H. F. Cserr, C. J. Harling-Berg, P. M. Knopf, Drainage of brain extracellular fluid into blood and deep cervical lymph and its immunological significance. *Brain pathology* **2**, 269-276 (1992).
4. R. O. Carare *et al.*, Solutes, but not cells, drain from the brain parenchyma along basement membranes of capillaries and arteries: significance for cerebral amyloid angiopathy and neuroimmunology. *Neuropathology and applied neurobiology* **34**, 131-144 (2008).
5. M. Johnston, A. Zakharov, C. Papaiconomou, G. Salmasi, D. Armstrong, Evidence of connections between cerebrospinal fluid and nasal lymphatic vessels in humans, non-human primates and other mammalian species. *Cerebrospinal Fluid Res* **1**, 2 (2004).
6. S. Kida, A. Pantazis, R. O. Weller, CSF drains directly from the subarachnoid space into nasal lymphatics in the rat. Anatomy, histology and immunological significance. *Neuropathology and applied neurobiology* **19**, 480-488 (1993).
7. J. N. Norwood *et al.*, Anatomical basis and physiological role of cerebrospinal fluid transport through the murine cribriform plate. *Elife* **8** (2019).
8. A. Aspelund *et al.*, A dural lymphatic vascular system that drains brain interstitial fluid and macromolecules. *The Journal of experimental medicine* **212**, 991-999 (2015).
9. J. H. Ahn *et al.*, Meningeal lymphatic vessels at the skull base drain cerebrospinal fluid. *Nature* **572**, 62-66 (2019).
10. M. Cifuentes, L. P. Fernandez, J. Perez, J. M. Perez-Figares, E. M. Rodriguez, Distribution of intraventricularly injected horseradish peroxidase in cerebrospinal fluid compartments of the rat spinal cord. *Cell and tissue research* **270**, 485-494 (1992).
11. H. J. Wagner, C. Pilgrim, J. Brandl, Penetration and removal of horseradish peroxidase injected into the cerebrospinal fluid: role of cerebral perivascular spaces, endothelium and microglia. *Acta neuropathologica* **27**, 299-315 (1974).
12. M. A. Lam *et al.*, The ultrastructure of spinal cord perivascular spaces: Implications for the circulation of cerebrospinal fluid. *Scientific reports* **7**, 12924 (2017).
13. Q. Ma, Y. Decker, A. Muller, B. V. Ineichen, S. T. Proulx, Clearance of cerebrospinal fluid from the sacral spine through lymphatic vessels. *The Journal of experimental medicine* **216**, 2492-2502 (2019).
14. R. Bozanovic-Sosic, R. Mollanji, M. G. Johnston, Spinal and cranial contributions to total cerebrospinal fluid transport. *American journal of physiology. Regulatory, integrative and comparative physiology* **281**, R909-916 (2001).
15. J. Leaston *et al.*, Do We Swallow the Waste From Our Brain? *Frontiers in neuroscience* **15**, 763780 (2021).
16. C. Kilkenny *et al.*, Animal research: reporting in vivo experiments: the ARRIVE guidelines. *Br J Pharmacol* **160**, 1577-1579 (2010).
17. X. Cai *et al.*, Imaging the effect of the circadian light-dark cycle on the glymphatic system in awake rats. *Proc Natl Acad Sci U S A* **117**, 668-676 (2020).
18. Q. Ma *et al.*, Rapid lymphatic efflux limits cerebrospinal fluid flow to the brain. *Acta neuropathologica* **137**, 151-165 (2019).
19. C. Gakuba *et al.*, General Anesthesia Inhibits the Activity of the "Glymphatic System". *Theranostics* **8**, 710-722 (2018).
20. E. Mathieu, N. Gupta, R. L. Macdonald, J. Ai, Y. H. Yucel, In vivo imaging of lymphatic drainage of cerebrospinal fluid in mouse. *Fluids Barriers CNS* **10**, 35 (2013).
21. S. M. Moinuddin, T. Tada, Study of cerebrospinal fluid flow dynamics in TGF-beta 1 induced chronic hydrocephalic mice. *Neurological research* **22**, 215-222 (2000).
22. S. Liu *et al.*, Fluid outflow in the rat spinal cord: the role of perivascular and paravascular pathways. *Fluids Barriers CNS* **15**, 13 (2018).
23. M. Miura, S. Kato, M. von Ludinghausen, Lymphatic drainage of the cerebrospinal fluid from monkey spinal meninges with special reference to the distribution of the epidural lymphatics. *Arch Histol Cytol* **61**, 277-286 (1998).
24. S. Antila *et al.*, Development and plasticity of meningeal lymphatic vessels. *The Journal of experimental medicine* **214**, 3645-3667 (2017).
25. L. Jacob *et al.*, Anatomy and function of the vertebral column lymphatic network in mice. *Nat Commun* **10**, 4594 (2019).
26. A. Verma *et al.*, Intrathecal (99m)Tc-DTPA imaging of molecular passage from lumbar cerebrospinal fluid to brain and periphery in humans. *Alzheimers Dement (Amst)* **12**, e12030 (2020).
27. K. Bechter, B. Schmitz, Cerebrospinal fluid outflow along lumbar nerves and possible relevance for pain research: case report and review. *Croat Med J* **55**, 399-404 (2014).

 doi:10.20944/preprints202211.0171.v1

28. Y. Inoue *et al.,* Integrated lymphography using fluorescence imaging and magnetic resonance imaging in intact mice. *Mol Imaging* **10**, 317-326 (2011).